

Azimuthal Anisotropy Scaling for Identified Mesons and Baryons: Insights into Medium Transport Properties, Equation of State and Hadronic Re-scattering

Roy A. Lacey^{1,*}

¹Department of Chemistry, Stony Brook University,
Stony Brook, NY, 11794-3400, USA

(Dated: October 8, 2024)

Azimuthal anisotropy scaling functions for identified mesons and baryons are derived from species-dependent measurements of the azimuthal anisotropy coefficients $v_2(p_T, \text{cent})$ and $v_3(p_T, \text{cent})$, in Pb+Pb collisions at $\sqrt{s_{NN}} = 2.76$ TeV and 5.02 TeV, Xe+Xe collisions at $\sqrt{s_{NN}} = 5.44$ TeV, and Au+Au collisions at $\sqrt{s_{NN}} = 0.2$ TeV. The scaling functions capture species-specific responses to radial flow and hadronic re-scattering, demonstrating consistency across flow- and jet-quenching-dominated p_T regions. These results provide robust constraints on fundamental transport properties of the quark-gluon plasma (QGP), including the specific shear viscosity η/s and the jet-quenching parameter \hat{q} , as well as insight into the centrality-dependent evolution of radial flow, a vital aspect of the system's dynamics. The findings reveal minimal influence from hadronic re-scattering at high beam energies and significant influence from re-scattering at lower energies. The centrality-dependent evolution of radial flow and the beam energy dependence of η/s offer new constraints on the equation of state (EOS) of the QGP, with important implications for advancing studies of QGP transport properties and heavy-ion collision dynamics.

PACS numbers: 25.75.-q, 25.75.Dw, 25.75.Ld

High-energy heavy-ion collisions at facilities such as the Large Hadron Collider (LHC) and the Relativistic Heavy Ion Collider (RHIC) provide invaluable laboratories for studying the quark-gluon plasma (QGP), a state of matter believed to replicate conditions just microseconds after the Big Bang [1–3]. Understanding the transport coefficients and the equation of state (EOS) of the QGP is crucial for elucidating its dynamics and thermodynamic properties.

Azimuthal anisotropy measurements are a key tool for probing the properties of the quark-gluon plasma (QGP). These measurements are typically quantified using complex coefficients V_n [4–6]:

$$V_n \equiv v_n e^{in\Psi_n} = \langle e^{in\phi} \rangle, \quad (1)$$

where v_n represents the magnitude of the azimuthal anisotropy, Ψ_n is the event-plane angle, and $\langle \cdot \rangle$ denotes averaging over the single-particle azimuthal distribution within an event.

The v_n coefficients can also be extracted using the Scalar Product (SP) method [7, 8], which employs a two-particle correlation technique based on the scalar product of the unit flow vector of a particle of interest, k , and the Q-vector of the event. The unit flow vector for particle k is defined as:

$$\mathbf{u}_{n,k} = \exp(in\varphi_k),$$

where φ_k is the azimuthal angle of the particle k . The Q-vector is calculated from a set of reference particles and is given by:

$$\mathbf{Q}_n = \sum w_i e^{in\varphi_i}, \quad (2)$$

where φ_i is the azimuthal angle of the i -th reference particle, n is the harmonic order, and w_i is a weight factor applied to

correct for non-uniform acceptance or efficiency of the reference particles. A pseudorapidity gap ($\Delta\eta$) is often introduced between the reference particles (sub-events A and B) used to construct the Q-vector and the particles of interest for which v_n is measured to suppress possible contributions from short-range correlations unrelated to QGP-driven anisotropy.

The v_n coefficients are then computed as:

$$v_n\{\text{SP}\} = \frac{\langle\langle \mathbf{u}_{n,k} \mathbf{Q}_n^* \rangle\rangle}{\sqrt{\frac{\langle\langle \mathbf{Q}_n \mathbf{Q}_n^A \rangle\rangle \langle\langle \mathbf{Q}_n \mathbf{Q}_n^B \rangle\rangle}{\langle\langle \mathbf{Q}_n^A \mathbf{Q}_n^{B*} \rangle\rangle}}}, \quad (3)$$

where the symbol $*$ denotes the complex conjugate. Single brackets $\langle \cdot \rangle$ denote an average over all events, while double brackets $\langle\langle \cdot \rangle\rangle$ indicate an average over all particles in all events. The denominator acts as a correction factor, accounting for the resolution of the \mathbf{Q}_n vector by balancing contributions from two independent sub-events A and B , thereby enhancing the precision of the anisotropy measurements.

Extensive research [9–41] has highlighted the impact of radial expansion, v_n -fluctuations, p_T -dependent viscous attenuation, jet quenching, and initial-state eccentricity (ε_n) on $v_n(p_T, \text{cent})$ measurements. These studies indicate that the coefficients $v_n(p_T, \text{cent})$ are fundamentally linked to collective flow dynamics for $p_T \lesssim 4 - 5$ GeV, while transitioning to jet quenching mechanisms at higher p_T .

Recently, anisotropy scaling functions [42] have been employed to unify diverse measurements [43–50] of $v_{2,3}(p_T, \text{cent})$ for charged particles across various transverse momentum and centrality ranges, providing essential insights into the initial-state eccentricity spectrum and the flow and jet-quenching characteristics of the medium created in heavy-ion collisions. These scaling functions constrained key transport properties such as the specific shear viscosity or viscosity-to-entropy ratio (η/s) and the medium's stopping power (\hat{q}).

However, they did not fully address the species-dependent differences in $v_n(p_T, \text{cent})$, which arise from particle identity. Understanding these differences is critical, as they can offer new constraints on (i) the underlying mechanisms governing particle production [51–59], (ii) the EOS, particularly through the species-dependent effects of radial flow [60], and (iii) the interplay between early-stage QGP-driven anisotropy and the late-stage dissipative hadronic rescattering that influences $v_n(p_T, \text{cent})$ [61].

The initial-state eccentricity and QGP transport properties, such as η/s , remain constant across all particle species for a given system at a fixed centrality. Therefore, species-specific differences in $v_n(p_T, \text{cent})$ primarily reflect their unique responses to radial flow and hadronic re-scattering. Radial flow, driven by QGP pressure gradients, imparts a mass-dependent “blue shift” in $v_n(p_T)$, where heavier particles experience a larger momentum boost due to their greater inertia. This effect results in a distinct mass ordering of $v_n(p_T)$ at low to intermediate p_T . A stiffer equation of state (EOS), with a higher pressure-to-energy density ratio, magnifies these blue shifts, especially for baryons. Consequently, species-dependent $v_n(p_T, \text{cent})$ measurements offer a valuable means to constrain the EOS by assessing how different particles respond to radial flow.

A key method for disentangling the contributions of the partonic and hadronic stages to anisotropic flow is to compare particles with small hadronic interaction cross-sections, such as the K^+ and ϕ mesons and the Ξ^\pm and Ω^\pm baryons, to particles like pions and protons, which undergo more substantial interactions in the hadronic medium. Particles with small hadronic interaction cross-sections, minimally affected by hadronic re-scattering, serve as baselines for probing the anisotropy developed during the partonic (QGP) phase. In contrast, particles with larger cross-sections experience significant modifications in the hadronic phase, resulting in differences in their v_n coefficients. By comparing the $v_n(p_T, \text{cent})$ of particles with minimal hadronic re-scattering to those with greater hadronic interactions, the role of hadronic re-scattering can be quantified. A significant difference in the flow coefficients between these groups signals substantial hadronic contributions. This comparative approach allows disentangling partonic and hadronic effects, refining the understanding of the QGP’s properties and the EOS.

This study extends the methodology for constructing anisotropy scaling functions [42] to identified mesons ($\pi^\pm, K^\pm, K_S^0, \phi$) and baryons (${}^3\text{He}, {}^2\text{H}, p, \Lambda^0, \Xi^-, \Omega^-$) and their antiparticles. The primary goal is not only to unify measurements of $v_2(p_T, \text{cent})$ and $v_3(p_T, \text{cent})$ across different transverse momentum and centrality ranges for these various particle species, but also to extract detailed information about species-specific responses to radial flow and hadronic rescattering via scaling. By constructing a scaling function that accounts for these factors, valuable insights can be obtained about the transport properties of the quark-gluon plasma (QGP) and the nuclear equation of state (EOS). The approach builds on foundational principles established for

charged hadrons, incorporating parameters such as initial-state eccentricities (ε_n), dimensionless system size ($\mathbb{R} \propto RT$), radial flow magnitude, the medium’s stopping power (\hat{q}), and the specific shear viscosity or viscosity-to-entropy ratio ($\eta/s \propto T^3/\hat{q}$), as well as the viscous correction to the thermal distribution function (δ_f) [13, 64].

These parameters define the anisotropy coefficients [35, 42, 65–67] as:

$$v_n(p_T, \text{cent}) = \varepsilon_n(\text{cent}) e^{-\frac{\beta}{\mathbb{R}}[n(n+\kappa p_T^2)]}, \quad n = 2, 3, \quad (4)$$

where $\beta \propto \eta/s$, $\delta_f = \kappa p_T^2$ [13, 35], and $\mathbb{R} \propto \langle N_{\text{chg}} \rangle_{|\eta| \leq 0.5}^{1/3}$ represents the dimensionless size related to mid-rapidity charged-particle multiplicity. The transition from flow to jet quenching at higher p_T is regulated by fixing the κp_T^2 term in Eq. 4, which remains constant for p_T values above approximately 4.5 GeV/c. This marks the threshold between flow-dominated and jet-quenching domains, ensuring a smooth transition across momentum regions while maintaining consistency between η/s and \hat{q} .

The scaling relationship correlating the harmonic $v_n(p_T, 0)$ measured in ultra-central events with $v'_n(p_T, \text{cent})$ at varying centralities, each associated with a specific \mathbb{R}' value, is given as [42]:

$$\frac{v_n(p_T, 0)}{\varepsilon_n(0)} e^{\frac{\eta\beta}{\mathbb{R}_0}[n+\kappa p_T^2]} = \frac{v'_n(p_T, \text{cent})}{\varepsilon'_n(\text{cent})} e^{\frac{\eta\beta}{\mathbb{R}_0}[n+\kappa p_T^2](\frac{\mathbb{R}_0}{\mathbb{R}'}-1)}. \quad (5)$$

For a given system at fixed centrality, $v_2(p_T, \text{cent})$ and $v_3(p_T, \text{cent})$, both influenced by the same underlying factors such as radial flow, η/s , and \hat{q} , are related as:

$$\frac{v_2(p_T, \text{cent})}{\varepsilon_2(\text{cent})} e^{\frac{2\alpha\beta}{\mathbb{R}_0}} = \left(\frac{v_3(p_T, \text{cent})}{\varepsilon_3(\text{cent})} \right)^{\frac{2}{3}}, \quad (6)$$

where α is a system-dependent but centrality-independent normalization constant reflecting potential differences in $\beta \propto \eta/s$ and system size.

In contrast to charged hadrons, which provide a species-averaged influence of radial flow and hadronic re-scattering, mesons (M) and baryons (B) exhibit species-specific responses that must be scaled separately. The $v'_2(p_T, \text{cent})$ coefficients for K^+ in 5.02 TeV Pb+Pb collisions serve as a baseline for quantifying both the difference in hadronic re-scattering and radial flow effects. K^+ mesons are ideal for this comparison because their intermediate mass makes them more sensitive to radial flow than lighter mesons like pions, while their reduced interaction with the hadronic medium provides a relatively clean reference point for hadronic re-scattering. This intermediate nature makes K^+ a balanced reference point for comparisons across species. Furthermore, comparisons between K^+ and baryons having significantly different hadronic interaction cross-sections provide corroborating insight into hadronic re-scattering. For a given system at a fixed centrality, the degree of hadronic re-scattering is estimated via scaling of the $v'_{2,3}(p_T, \text{cent})$ coefficients for pions to the scaled baseline as:

$$\frac{v'_n(p_T)}{\varepsilon'_n} e^{\frac{\eta\beta'}{\mathbb{R}_0}[n+\kappa p_T^2](\frac{\mathbb{R}_0}{\mathbb{R}'}-1)} = \left(\frac{v''_n(p_T)}{\varepsilon''_n} \right)^{\zeta_M} e^{\frac{\eta\beta\zeta_M}{\mathbb{R}_0}[n+\kappa p_T^2](\frac{\mathbb{R}_0}{\mathbb{R}'}-1)}, \quad (7)$$

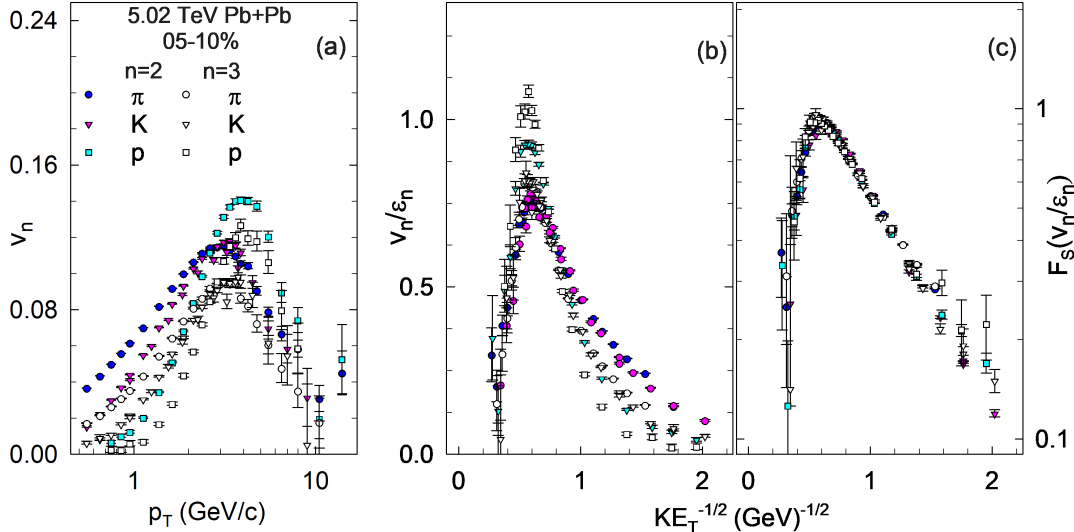


FIG. 1. (Color Online) Comparison of the $v_2(p_T)$ and $v_3(p_T)$ coefficients for π , K and p in panel (a), their eccentricity-scaled values v_2/ε_2 and v_3/ε_3 in panel (b), and the resulting scaling function in panel (c) for 5-10% central Pb+Pb collisions at 5.02 TeV. The data are sourced from the ALICE collaboration [62, 63].

and

$$\frac{v'_2(p_T, \text{cent})}{\varepsilon'_2(\text{cent})} e^{\frac{2\alpha\beta'}{\mathbb{R}_0}} = \left(\frac{v_3(p_T, \text{cent})}{\varepsilon_3(\text{cent})} \right)^{\frac{2}{3}\zeta_M}, \quad (8)$$

where β' characterizes η/s for the baseline, $\zeta_M = (1 - \zeta_h)$ and ζ_h quantifies possible differences in hadronic re-scattering.

The radial flow is similarly estimated by scaling the $v_{2,3}(p_T, \text{cent})$ coefficients for baryons to the scaled baseline as:

$$\frac{v'_n(p_T)}{\varepsilon'_n} e^{\frac{n\beta'}{\mathbb{R}_0} [n + \kappa p_T^2] (\frac{\mathbb{R}_0}{\mathbb{R}'_0} - 1)} = e^{-n_B \zeta_B \frac{2\beta}{\alpha \mathbb{R}_0}} \left(\frac{v'''_n(p_T)}{\varepsilon'''_n} \right)^{\zeta_B} e^{\frac{n\beta\zeta_r}{\mathbb{R}_0} [n + \kappa p_T^2] (\frac{\mathbb{R}_0}{\mathbb{R}'_0} - 1)}, \quad (9)$$

and

$$\frac{v'_2(p_T, \text{cent})}{\varepsilon'_2(\text{cent})} e^{\frac{2\alpha\beta'}{\mathbb{R}_0}} = e^{-2n_B \zeta_B \frac{2\alpha\beta}{\mathbb{R}_0}} \left(\frac{v_3(p_T, \text{cent})}{\varepsilon_3(\text{cent})} \right)^{\frac{2}{3}\zeta_B}, \quad (10)$$

where n_B is the baryon number, $\zeta_B = (1 - \zeta_r)^{n_B}$ and ζ_r parametrizes the difference in the influence of radial flow between baryons and the baseline.

The scaled anisotropy coefficients for each particle species are plotted versus transverse kinetic energy, $KE_T = \left(\sqrt{p_T^2 + m_0^2} - m_0 \right)$, where m_0 is the rest mass of the respective particle species. This choice of plotting against KE_T normalizes the inertia between particle species, effectively minimizing mass-dependent effects and enabling a more straightforward comparison of the anisotropy coefficients across species. This method, referred to as KE_T scaling, allows for a more consistent analysis of species-specific responses to radial flow and hadronic re-scattering.

Equations 7 - 10 offer a comprehensive scaling framework for understanding anisotropy coefficients across a broad spectrum of particle species, shedding light on the underlying QGP properties, EOS, and hadronic re-scattering.

The data used in this study are sourced from the ALICE, PHENIX and STAR collaborations, consisting of $v_2(p_T, \text{cent})$ and $v_3(p_T, \text{cent})$ measurements for identified particle species in Pb+Pb collisions at $\sqrt{s_{NN}} = 2.76$ TeV [69–72] and 5.02 TeV [62, 63, 68], Xe+Xe collisions at 5.44 TeV [73], and Au+Au collisions at 0.2 TeV [74–76]. The reported v_n values represent an average over particles and anti-particles as the differences between them were within the uncertainty of the measurements. Centrality-dependent charged-particle multiplicities, $\langle N_{\text{chg}} \rangle_{|\eta| \leq 0.5}$, were extracted from corresponding multiplicity density measurements [77–81]. A previously established value of $\kappa = 0.17 (\text{GeV}/c)^{-2}$ [35] was used to compute the viscous correction, δf .

Eccentricities were calculated using the Monte Carlo quark-Glauber model (MC-qGlauber) [35], which builds on the MC-Glauber framework [82, 83] by incorporating quark substructure, quark distributions within nucleons, and cross sections that reproduce the nucleon-nucleon inelastic cross-section at various beam energies. This model accounts for the nucleon's finite size and wounding profile. Simulations were performed for Au and Pb nuclei and Xe nuclei with different initial-state deformations, characterized by the deformation parameter β_2 . The estimated systematic eccentricity uncertainty due to model parameter variations is approximately 2–3%. A selection of these eccentricities, as a function of centrality, are reported in Ref. [42].

The scaling function was derived from the species-dependent differential measurements $v_2(p_T, \text{cent})$ and

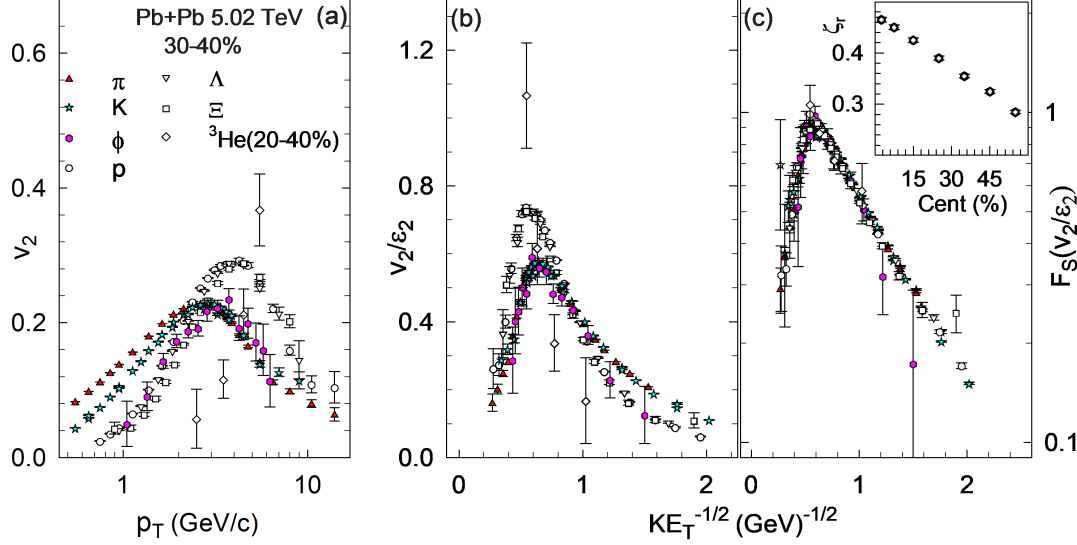


FIG. 2. (Color Online) Comparison of $v_2(p_T)$ for the mesons π , K , K_S^0 , ϕ and baryons p , Λ^0 , Ξ , ${}^3\text{He}$ in panel (a), their eccentricity-scaled values v_2/ε_2 in panel (b), and the resulting scaling function in panel (c) for 30-40% central Pb+Pb collisions at 5.02 TeV. The inset in panel (c) shows the centrality dependence of ζ_r , which parametrizes the radial flow response across the full centrality span. The data are sourced from the ALICE collaboration [62, 63, 68].

$v_3(p_T, \text{cent})$ at each centrality using equations 7 - 10. Figure 1 illustrates the scaling procedure for 5-10% central Pb+Pb collisions at 5.02 TeV, with $1/\sqrt{KE_T}$ plotted on the x-axis in panels (b) and (c) to highlight the flow- and jet-quenching-dominated regions [14, 84]. Panel (a) shows the species-dependent differences in $v_2(p_T)$ and $v_3(p_T)$, along with the relative difference between them for each species. Panel (b) demonstrates that eccentricity scaling [$v_n(p_T)/\varepsilon_n$], combined with KE_T scaling, significantly improves agreement between species—especially for pions and kaons—but still falls short of fully capturing all species-dependent variations. Panel (c) presents the final scaling function, illustrating data convergence onto a single curve across both flow- and jet-quenching-dominated domains for $\alpha = 1$, $\beta = 0.88$, $\zeta_h = 0.00$, and $\zeta_r = 0.45$. These values suggest that the flow coefficients in Pb+Pb collisions at 5.02 TeV are primarily influenced by the quark-gluon plasma's specific viscosity and radial flow (QGP), with minimal contributions from hadronic re-scattering. Figure 2 shows a similar scaling procedure for $v_2(p_T)$ for mesons π , K , K_S^0 , ϕ and baryons p , Λ^0 , Ξ , ${}^3\text{He}$ in 30-40% central Pb+Pb collisions at 5.02 TeV. Despite their differing hadronic interaction cross-sections, the resulting scaling function obtained for $\alpha = 1$, $\beta = 0.88$, $\zeta_h = 0.00$, and $\zeta_r = 0.355$ suggests that hadronic re-scattering remains minimal, while the blue shift for baryons decreases in more peripheral collisions, reflecting the expected reduction in radial flow with decreasing energy density.

Validation of the scaling function was performed across the full centrality range (0.0-0.1% to 50-60%) using fixed parameters ($\alpha = 1$, $\beta = 0.88$, and $\zeta_h = 0.00$), with variations in ζ_r , which quantifies the species-specific radial flow response, as

shown in the inset of Fig. 2. The scaling coefficients for the 0-5% centrality cut represent an average that incorporates values from both ultra-central and non-ultra-central collisions, capturing contributions from both regimes. The inset indicates an increase in ζ_r as collisions become more central, reflecting an increasing influence of radial flow. This centrality-dependent scaling could provide crucial constraints on the stiffness of the equation of state (EOS). This validation provides robust evidence for the consistency of the scaling coefficients and supports the reliability of the derived eccentricity spectrum and its ratios while offering insight into the evolution of radial flow with centrality.

Similarly, robust scaling functions, closely matching those for Pb+Pb collisions at 5.02 TeV, were obtained across the full range of species-dependent $v_2(p_T, \text{cent})$ and $v_3(p_T, \text{cent})$ measurements for Xe+Xe collisions at 5.44 TeV, Pb+Pb collisions at 2.76 TeV, and Au+Au collisions at 0.2 TeV. Figs. 3 and 4 show representative scaling illustrations for 20-30% central Pb+Pb and 0-30% central Au+Au collisions, respectively. The scaling functions were obtained using the fixed parameters ($\alpha = 1$, $\beta = 0.84$, and $\zeta_h = 0.00$) for Pb+Pb, and ($\alpha = 1.6$, $\beta = 0.55$, and $\zeta_h = 0.05$) with variations in ζ_r , as shown in the insets of Figs. 3 and 4. These values suggest that the flow coefficients in Pb+Pb collisions at 2.76 TeV are primarily influenced by the quark-gluon plasma's specific viscosity and radial flow (QGP), with minimal contributions from hadronic re-scattering. A small decrease in η/s ($\sim 5\%$) was observed, but the radial flow magnitude remains comparable to that observed in Pb+Pb collisions at 5.02 TeV. The trend in the centrality dependence of ζ_r is consistent across Xe+Xe, Pb+Pb and Au+Au collisions, as demonstrated in the insets of Figs.

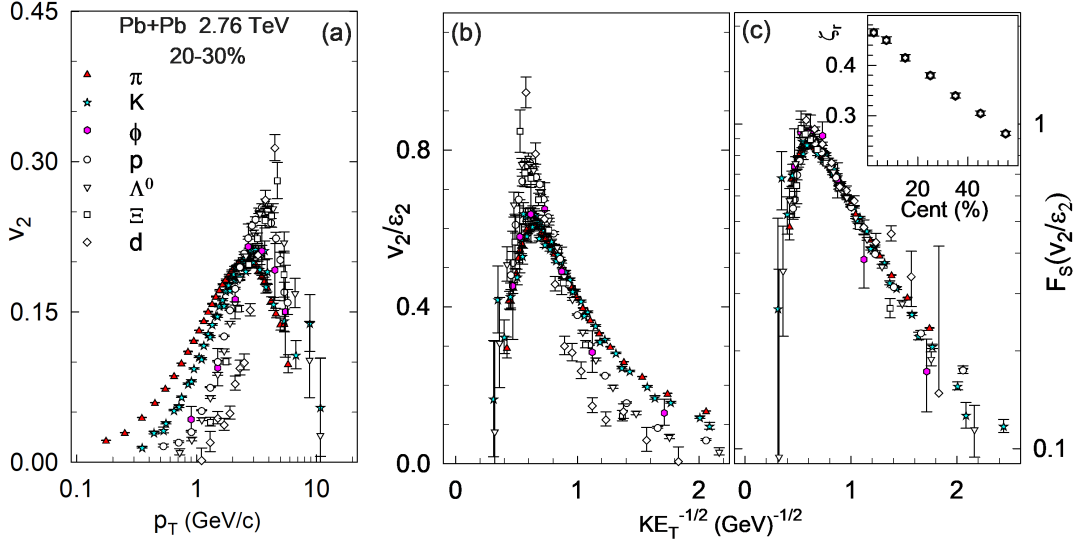


FIG. 3. (Color Online) Comparison of $v_2(p_T)$ for the mesons π, K, K_S^0, ϕ and baryons p, Λ^0, Ξ, d in panel (a), their eccentricity- scaled values v_2/ε_2 in panel (b), and the resulting scaling function in panel (c) for 20-30% central Pb+Pb collisions at 2.76 TeV. The inset in panel (c) shows the centrality dependence of ζ_r , which parametrizes the radial flow response across the full centrality span. The data are sourced from the ALICE collaboration [69–72].

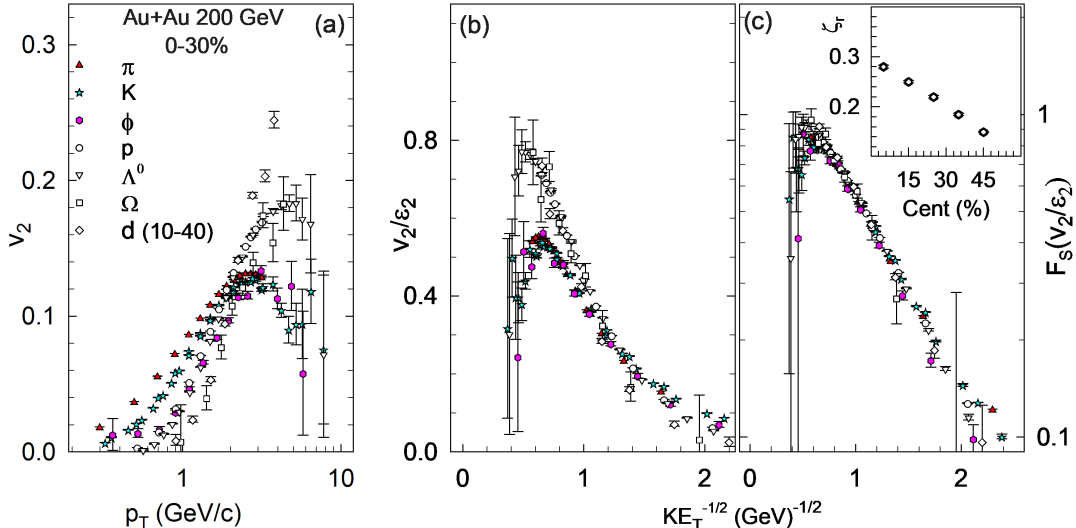


FIG. 4. (Color Online) Comparison of $v_2(p_T)$ for the mesons π, K, K_S^0, ϕ and baryons p, Λ^0, Ω, d in panel (a), their eccentricity-scaled values v_2/ε_2 in panel (b), and the resulting scaling function in panel (c) for 0-30% central Au+Au collisions at 0.20 TeV. The inset in panel (c) shows the centrality dependence of ζ_r , which parametrizes the radial flow response across the full centrality span. The data are sourced from the PHENIX and STAR collaborations [74–76].

2, 3, and 4 for Pb+Pb and Au+Au collisions. The results for Xe+Xe collisions at 5.44 TeV closely follow the trend seen in Pb+Pb collisions, with slightly lower implied radial flow due to the smaller system size. In contrast, the scaling coefficients for Au+Au suggest significant reductions in η/s ($\sim 37\%$) and radial flow ($\sim 60\%$), along with contributions from hadronic re-scattering when the beam energy is reduced from 5.02 TeV to 0.2 TeV.

The newly derived scaling functions for identified mesons and baryons extend the foundational insights previously obtained for charged hadrons, offering robust constraints on both the shear viscosity to entropy ratio (η/s) and the jet-quenching parameter (\hat{q}). By maintaining consistency across both flow and jet-quenching domains, these functions reinforce the relationship between η/s and T^3/\hat{q} , as initially proposed by Majumder et al. [64, 85]. This work also introduces species-

specific radial flow responses, captured by ζ_r , which add new constraints on the stiffness of the equation of state (EOS) and the transport properties of the quark-gluon plasma (QGP).

The smooth transition observed between the low and high p_T regions—where collective flow dominates at lower p_T and jet quenching becomes significant at higher p_T —provides crucial insights into the relative magnitudes of η/s and \hat{q} [13]. This transition highlights the influence of path length and radiative energy loss in shaping high p_T anisotropy, which depends on the dimensionless system size, $\mathbb{R} \propto \langle N_{\text{chg}} \rangle^{1/3}$.

Furthermore, utilizing the δf formalism [13], preliminary findings suggest that η/s exceeds T^3/\hat{q} , supporting the view of the QGP as a strongly coupled plasma. This low shear viscosity and moderate stopping power balance facilitates strong collective flow and jet quenching at higher p_T [85]. These results underscore the critical role of radial flow in determining the QGP's dynamical properties and provide a vital framework for future studies on the EOS and transport coefficients in heavy-ion collisions.

This study presents a comprehensive framework for anisotropy scaling functions, extending their application to identified mesons and baryons in heavy-ion collisions. By analyzing species-dependent measurements of $v_2(p_T, \text{cent})$ and $v_3(p_T, \text{cent})$, the scaling functions, which exhibit consistency across the p_T domains for flow- and jet-quenching, reveal key insights into the centrality-dependent evolution of radial flow and the beam energy dependence of the specific shear viscosity η/s in the quark-gluon plasma (QGP). Minimal hadronic re-scattering effects are observed at high beam energies, while significant re-scattering is evident in lower energy collisions. Comparisons between Pb+Pb, Xe+Xe, and Au+Au collisions indicate robust constraints on the equation of state (EOS) of the QGP. These results underscore the critical role of shear viscosity, radiative energy loss, radial flow, and hadronic re-scattering in shaping azimuthal anisotropy patterns, reinforcing a crucial foundation for future studies into QGP transport properties and collision dynamics.

Phys. Rev. Lett. **106**, 192301 (2011), [Erratum: *Phys. Rev. Lett.* 109, 139904 (2012)], arXiv:1011.2783 [nucl-th].

- [10] B. Alver *et al.* (PHOBOS), *Phys. Rev. C* **77**, 014906 (2008), arXiv:0711.3724 [nucl-ex].
- [11] B. Alver *et al.* (PHOBOS), *Phys. Rev. C* **81**, 034915 (2010), arXiv:1002.0534 [nucl-ex].
- [12] J.-Y. Ollitrault, A. M. Poskanzer, and S. A. Voloshin, *Phys. Rev. C* **80**, 014904 (2009), arXiv:0904.2315 [nucl-ex].
- [13] K. Dusling, G. D. Moore, and D. Teaney, *Phys. Rev. C* **81**, 034907 (2010), arXiv:0909.0754 [nucl-th].
- [14] R. A. Lacey, A. Taranenko, R. Wei, N. Ajitanand, J. Alexander, *et al.*, *Phys. Rev. C* **82**, 034910 (2010), arXiv:1005.4979 [nucl-ex].
- [15] C. Shen, U. Heinz, P. Huovinen, and H. Song, *Phys. Rev. C* **84**, 044903 (2011), arXiv:1105.3226 [nucl-th].
- [16] H. Niemi, G. S. Denicol, H. Holopainen, and P. Huovinen, *Phys. Rev. C* **87**, 054901 (2013), arXiv:1212.1008 [nucl-th].
- [17] J. Fu, *Phys. Rev. C* **92**, 024904 (2015).
- [18] C. Andrés, J. Dias de Deus, A. Moscoso, C. Pajares, and C. A. Salgado, *EPJ Web Conf.* **90**, 08003 (2015).
- [19] M. Abdallah *et al.* (STAR), *Phys. Rev. Lett.* **129**, 252301 (2022), arXiv:2201.10365 [nucl-ex].
- [20] J. Adam *et al.* (STAR), *Phys. Lett. B* **783**, 459 (2018), arXiv:1803.03876 [nucl-ex].
- [21] J. Adam *et al.* (ALICE), *Phys. Rev. Lett.* **117**, 182301 (2016), arXiv:1604.07663 [nucl-ex].
- [22] Z. Qiu and U. W. Heinz, *Phys. Rev. C* **84**, 024911 (2011), arXiv:1104.0650 [nucl-th].
- [23] A. Adare *et al.* (PHENIX), *Phys. Rev. Lett.* **107**, 252301 (2011), arXiv:1105.3928 [nucl-ex].
- [24] N. Magdy (STAR), *Proceedings, 27th International Conference on Ultrarelativistic Nucleus-Nucleus Collisions (Quark Matter 2018): Venice, Italy, May 14-19, 2018*, *Nucl. Phys.* **A982**, 255 (2019), arXiv:1807.07638 [nucl-ex].
- [25] L. Adamczyk *et al.* (STAR), *Phys. Rev. C* **94**, 034908 (2016), arXiv:1601.07052 [nucl-ex].
- [26] L. Adamczyk *et al.* (STAR), *Phys. Rev. C* **93**, 014907 (2016), arXiv:1509.08397 [nucl-ex].
- [27] L. Adamczyk *et al.* (STAR), *Phys. Rev. Lett.* **115**, 222301 (2015).
- [28] L. Adamczyk *et al.* (STAR), *Phys. Rev. Lett.* **116**, 112302 (2016), arXiv:1601.01999 [nucl-ex].
- [29] J. Adam *et al.* (STAR), *Phys. Rev. Lett.* **122**, 172301 (2019), arXiv:1901.08155 [nucl-ex].
- [30] F. G. Gardim, J. Noronha-Hostler, M. Luzum, and F. Grassi, *Phys. Rev. C* **91**, 034902 (2015), arXiv:1411.2574 [nucl-th].
- [31] H. Holopainen, H. Niemi, and K. J. Eskola, *Phys. Rev. C* **83**, 034901 (2011), arXiv:1007.0368 [hep-ph].
- [32] G.-Y. Qin, H. Petersen, S. A. Bass, and B. Muller, *Phys. Rev. C* **82**, 064903 (2010), arXiv:1009.1847 [nucl-th].
- [33] C. Gale, S. Jeon, B. Schenke, P. Tribedy, and R. Venugopalan, *Phys. Rev. Lett.* **110**, 012302 (2013), arXiv:1209.6330 [nucl-th].
- [34] K. M. Burke *et al.* (JET), *Phys. Rev. C* **90**, 014909 (2014), arXiv:1312.5003 [nucl-th].
- [35] P. Liu and R. A. Lacey, *Phys. Rev. C* **98**, 021902 (2018), arXiv:1802.06595 [nucl-ex].
- [36] K. Adcox *et al.* (PHENIX), *Phys. Rev. Lett.* **88**, 022301 (2002), arXiv:nucl-ex/0109003.
- [37] C. Adler *et al.* (STAR), *Phys. Rev. Lett.* **89**, 202301 (2002), arXiv:nucl-ex/0206011.
- [38] H.-z. Zhang, J. F. Owens, E. Wang, and X. N. Wang, *J. Phys. G* **35**, 104067 (2008), arXiv:0804.2381 [hep-ph].
- [39] B. Abelev *et al.* (ALICE), *JHEP* **03**, 013 (2014),

* E-mail: Roy.Lacey@Stonybrook.edu

- [1] E. V. Shuryak, *Phys. Rept.* **115**, 151 (1984).
- [2] S. A. Bass, M. Gyulassy, H. Stoecker, and W. Greiner, *J. Phys. G* **25**, R1 (1999), arXiv:hep-ph/9810281.
- [3] H. Satz, *Rept. Prog. Phys.* **63**, 1511 (2000), arXiv:hep-ph/0007069.
- [4] A. Bilandzic, R. Snellings, and S. Voloshin, *Phys. Rev. C* **83**, 044913 (2011), arXiv:1010.0233 [nucl-ex].
- [5] M. Luzum, *J. Phys. G* **38**, 124026 (2011), arXiv:1107.0592 [nucl-th].
- [6] D. Teaney and L. Yan, *Phys. Rev. C* **86**, 044908 (2012), arXiv:1206.1905 [nucl-th].
- [7] C. Adler *et al.* (STAR), *Phys. Rev. C* **66**, 034904 (2002), arXiv:nucl-ex/0206001 [nucl-ex].
- [8] S. A. Voloshin, A. M. Poskanzer, and R. Snellings, *Landolt-Bornstein* **23**, 293 (2010), arXiv:0809.2949 [nucl-ex].
- [9] H. Song, S. A. Bass, U. Heinz, T. Hirano, and C. Shen,

- arXiv:1311.0633 [nucl-ex].
- [40] Y. Mehtar-Tani, J. G. Milhano, and K. Tywoniuk, *Int. J. Mod. Phys. A* **28**, 1340013 (2013), arXiv:1302.2579 [hep-ph].
- [41] G.-Y. Qin and X.-N. Wang, *Int. J. Mod. Phys. E* **24**, 1530014 (2015), arXiv:1511.00790 [hep-ph].
- [42] R. A. Lacey, (2024), arXiv:2402.09389 [nucl-ex].
- [43] K. Aamodt *et al.* (ALICE), *Phys. Rev. Lett.* **105**, 252302 (2010), arXiv:1011.3914 [nucl-ex].
- [44] G. Aad *et al.* (ATLAS), *Phys. Lett. B* **707**, 330 (2012), arXiv:1108.6018 [hep-ex].
- [45] G. Aad *et al.* (ATLAS), *Phys. Rev. C* **86**, 014907 (2012), arXiv:1203.3087 [hep-ex].
- [46] S. Chatrchyan *et al.* (CMS), *Eur. Phys. J. C* **72**, 2012 (2012), arXiv:1201.3158 [nucl-ex].
- [47] S. Chatrchyan *et al.* (CMS), *Phys. Rev. C* **87**, 014902 (2013), arXiv:1204.1409 [nucl-ex].
- [48] K. Aamodt *et al.* (ALICE), *Phys. Rev. Lett.* **107**, 032301 (2011), arXiv:1105.3865 [nucl-ex].
- [49] G. Aad *et al.* (ATLAS), *JHEP* **11**, 183 (2013), arXiv:1305.2942 [hep-ex].
- [50] S. Chatrchyan *et al.* (CMS), *Phys. Rev. C* **89**, 044906 (2014), arXiv:1310.8651 [nucl-ex].
- [51] S. A. Voloshin, *Nucl. Phys. A* **715**, 379 (2003), arXiv:nucl-ex/0210014.
- [52] D. Molnar and S. A. Voloshin, *Phys. Rev. Lett.* **91**, 092301 (2003), arXiv:nucl-th/0302014.
- [53] A. Adare *et al.* (PHENIX), *Phys. Rev. C* **85**, 064914 (2012), arXiv:1203.2644 [nucl-ex].
- [54] A. Adare *et al.* (PHENIX), *Phys. Rev. Lett.* **98**, 162301 (2007), arXiv:nucl-ex/0608033.
- [55] J. Adams *et al.* (STAR), *Phys. Rev. Lett.* **92**, 052302 (2004), arXiv:nucl-ex/0306007.
- [56] B. I. Abelev *et al.* (STAR), *Phys. Rev. C* **75**, 054906 (2007), arXiv:nucl-ex/0701010.
- [57] J. Adams *et al.* (STAR), *Phys. Rev. C* **72**, 014904 (2005), arXiv:nucl-ex/0409033.
- [58] S. S. Adler *et al.* (PHENIX), *Phys. Rev. Lett.* **91**, 182301 (2003), arXiv:nucl-ex/0305013.
- [59] S. Afanasiev *et al.* (PHENIX), *Phys. Rev. Lett.* **99**, 052301 (2007), arXiv:nucl-ex/0703024.
- [60] P. Huovinen, P. F. Kolb, U. W. Heinz, P. V. Ruuskanen, and S. A. Voloshin, *Phys. Lett. B* **503**, 58 (2001), arXiv:hep-ph/0101136.
- [61] T. Hirano, U. W. Heinz, D. Kharzeev, R. Lacey, and Y. Nara, *Phys. Lett. B* **636**, 299 (2006), arXiv:nucl-th/0511046 [nucl-th].
- [62] Y. Zhu (ALICE), *PoS ICHEP2018*, 441 (2019).
- [63] S. Acharya *et al.* (ALICE), *JHEP* **05**, 243 (2023), arXiv:2206.04587 [nucl-ex].
- [64] A. Majumder, B. Muller, and X.-N. Wang, *Phys. Rev. Lett.* **99**, 192301 (2007), arXiv:hep-ph/0703082.
- [65] P. Staig and E. Shuryak, *Phys. Rev. C* **84**, 034908 (2011), arXiv:1008.3139 [nucl-th].
- [66] S. S. Gubser and A. Yarom, *Nucl. Phys. B* **846**, 469 (2011), arXiv:1012.1314 [hep-th].
- [67] R. A. Lacey, Y. Gu, X. Gong, D. Reynolds, N. N. Ajitanand, J. M. Alexander, A. Mwai, and A. Taranenko, (2013), arXiv:1301.0165 [nucl-ex].
- [68] S. Acharya *et al.* (ALICE), *Phys. Rev. C* **102**, 055203 (2020), arXiv:2005.14639 [nucl-ex].
- [69] B. B. Abelev *et al.* (ALICE), *JHEP* **06**, 190 (2015), arXiv:1405.4632 [nucl-ex].
- [70] J. Adam *et al.* (ALICE), *JHEP* **09**, 164 (2016), arXiv:1606.06057 [nucl-ex].
- [71] S. Acharya *et al.* (ALICE), *Eur. Phys. J. C* **77**, 658 (2017), arXiv:1707.07304 [nucl-ex].
- [72] S. Acharya *et al.* (ALICE), *Phys. Lett. B* **784**, 82 (2018), arXiv:1805.01832 [nucl-ex].
- [73] S. Acharya *et al.* (ALICE), *JHEP* **10**, 152 (2021), arXiv:2107.10592 [nucl-ex].
- [74] A. Adare *et al.* (PHENIX), *Phys. Rev. C* **93**, 051902 (2016), arXiv:1412.1038 [nucl-ex].
- [75] L. Adamczyk *et al.* (STAR), *Phys. Rev. Lett.* **116**, 062301 (2016), arXiv:1507.05247 [nucl-ex].
- [76] M. Abdallah *et al.* (STAR), *Phys. Rev. C* **105**, 064911 (2022), arXiv:2203.07204 [nucl-ex].
- [77] K. Aamodt *et al.* (ALICE), *Phys. Rev. Lett.* **106**, 032301 (2011), arXiv:1012.1657 [nucl-ex].
- [78] J. Adam *et al.* (ALICE), *Phys. Rev. Lett.* **116**, 222302 (2016), arXiv:1512.06104 [nucl-ex].
- [79] S. Acharya *et al.* (ALICE), *Phys. Lett. B* **790**, 35 (2019), arXiv:1805.04432 [nucl-ex].
- [80] A. M. Sirunyan *et al.* (CMS), *Phys. Lett. B* **799**, 135049 (2019), arXiv:1902.03603 [hep-ex].
- [81] R. A. Lacey, P. Liu, N. Magdy, M. Csanad, B. Schweid, N. N. Ajitanand, J. Alexander, and R. Pak, (2016), arXiv:1601.06001 [nucl-ex].
- [82] M. L. Miller, K. Reygers, S. J. Sanders, and P. Steinberg, *Ann. Rev. Nucl. Part. Sci.* **57**, 205 (2007), arXiv:nucl-ex/0701025.
- [83] B. Alver *et al.* (PHOBOS), *Phys. Rev. Lett.* **98**, 242302 (2007), arXiv:nucl-ex/0610037.
- [84] Y. L. Dokshitzer and D. E. Kharzeev, *Phys. Lett. B* **519**, 199 (2001), arXiv:hep-ph/0106202.
- [85] D. Everett *et al.* (JETSCAPE), *Phys. Rev. C* **103**, 054904 (2021), arXiv:2011.01430 [hep-ph].